On the Structural Organization of Isolated Bovine Lens Fiber Junctions

G. ZAMPIGHI, S. A. SIMON, J. D. ROBERTSON, T. J. McINTOSH, and M. J. COSTELLO
Departments of Anatomy, Anesthesiology, and Physiology, Duke University Medical Center, Durham, North Carolina 27710. Dr. Zampighi's present address is the Department of Anatomy and The Jerry Lewis Neuromuscular Research Center, University of California at Los Angeles School of Medicine, Los Angeles, California 90024.

ABSTRACT Junctions between fiber cells of bovine lenses have been isolated in milligram quantities without using detergents or proteases. The structure of the isolated junctions has been studied by thin-section, negative-stain, and freeze-fracture electron microscopy and by x-ray diffraction. The junctions are large and most often have an undulating surface topology as determined by thin sectioning and freeze-fracture. These undulations resemble the tongue-and-groove interdigitations between lens fiber cells previously seen by others (D. H. Dickson and G. W. Crock, 1972, *Invest. Ophthalmol.* 11:809–815). In sections, the isolated junctions display a pentalamellar structure ~13–14 nm in overall thickness, which is significantly thinner than liver gap junctions. Each junctional membrane contains in the plane of the lipid bilayers distinct units arranged in a square lattice with a center-to-center spacing of 6.6 nm. Freeze-fracture replicas of the junctions fractured transversely show that the repeating units extend across the entire thickness of each membrane. Each unit is probably constructed from four identical subunits, with each subunit containing a protein of an apparent molecular weight of 27,000.

We conclude that the lens junctions are structurally and chemically different from gap junctions and could represent a new kind of intercellular contact, not simply another crystalline state of the gap junction protein.

Mammalian lens fiber cells have been found by electron microscopy to contain extensive junctions usually considered to be of the communicating ("gap" or "nexus") type (2, 3, 18, 24, 26, 27, 30, 38, 43, 50) that mediate and regulate electrical and metabolic coupling (19, 45). These junctions have been studied extensively by morphological (18, 24–27, 39, 41, 42), chemical (2, 3, 5–8, 23, 36, 47), and immunological techniques (4, 8, 22, 57). Although there is good agreement regarding their chemical composition, their molecular organization is still controversial. For example, at least four packing arrangements of the morphological subunits composing the junctions have been described. Among these are hexagonal (3, 23, 39), rhomboidal (41, 42), and orthogonal (24, 41, 42) crystalline lattices, as well as the most frequently described aperiodic (random) packing of morphological subunits (2, 7, 17, 23, 39, 41, 42). It has been suggested that transitions between the random state and one of the crystalline lattices may be induced by changing the ionic milieu (39, 41, 42), although the extent of these transitions remains controversial (17, 23). Moreover, by analogy with other junctions (40), it has been proposed that the random and crystalline packing arrangements represent, respectively, coupled and uncoupled states of the junctions (39, 41, 42).

In this paper, we present results of chemical and structural studies of bovine lens junctions obtained from a pure junction fraction isolated without using detergents or proteases. The isolated junctions are seen as pentalamellar structures 13–14 nm in overall thickness. Each junctional membrane contains extensive two-dimensional square arrays of units with a center-to-center spacing of 6.6 nm. Each structural unit appears to span the entire thickness of the bilayer. The fraction contains one major protein with an apparent molecular weight of 27,000.

An important conclusion is that the isolated lens junctions we describe are structurally different from gap junctions. Our findings suggest that the square junctions may represent a separate class of intercellular contact.

MATERIALS AND METHODS

Bovine lenses were either obtained from a local slaughterhouse or frozen from Pel-Freeze Biologicals (Rogers, AR). The lenses that had been excised from the eyes at the slaughterhouse were kept on ice in solution A (2 mM $NaHCO_3$, 3 mM

THE JOURNAL OF CELL BIOLOGY · VOLUME 93 APRIL 1982 175–189

EDTA, and 100 μM phenylmethylsulfonyl fluoride adjusted to pH 8.0 with NaOH) until the isolation procedure commenced ~2 h later. The frozen lenses were thawed slowly to room temperature at which they were transparent and pliable. Lenses that remained hard (presumably from older animals) were discarded. In one experiment, the freshly obtained lenses were separated into two groups: one was kept on ice, whereas the other was frozen in dry ice at the slaughterhouse and later slowly thawed. Subsequent chemical and morphological analyses showed no differences between the two groups. Therefore, the data obtained from fresh and frozen lenses will be presented together.

Isolation

In a typical experiment, we used ~30 lenses from which the capsule as well as several outer layers of cortical fibers were removed. Unless otherwise noted, all isolation procedures were performed at 4°C. Following a procedure similar to the one outlined by Goodenough (18), the fibers were resuspended in 200 ml of solution A and homogenized by hand in a Dounce glass homogenizer with a Teflon pestle that was machined to provide a looser fit than the factory clearance. Usually 10 strokes were necessary to homogenize the fibers. The resulting suspension of broken cells was diluted to 1.8 liters with solution A, left for 10 min, twice-filtered through four layers of surgical gauze, and then passed through two layers of 50-mesh nylon. The suspension was centrifuged at 2,000 g for 10 min (Sorvall GSA rotor; Dupont Instruments, Wilmington, DE). The pellet was homogenized, diluted, and centrifuged again under the same conditions. Pigmented cells were eliminated by collecting only the white portion of the pellet.

The pellets were resuspended in 1.8 liters of solution B (4 mM Tris, 5 mM EDTA, 1 mM $CaCl_2$, 1.5 mM NaN_3, pH 8). The suspension was centrifuged at 2,000 g for 20 min (Sorvall GSA rotor). The free calcium concentration in solution B was calculated to be 1.6×10^{-8} M using a K_D of 3.23×10^{-8} M (44). The pellet was resuspended in 300 ml of 4 M urea in solution B and centrifuged at 17,000 g for 10 min (Sorvall GSA rotor). The resulting pellet was resuspended in 150 ml of 7 m urea in solution B and centrifuged at 64,000 g for 100 min (Type 60 Ti rotor; Beckman Instruments, Palo Alto, CA). The white portion of the pellet was resuspended in solution B and the sucrose concentration was increased to 47-48% by adding 67% sucrose in solution B. A discontinuous density gradient composed of 41/25/8% sucrose, all in solution B, was layered on top and the tubes were centrifuged at 97,000 g for 30 min (Beckman SW-28 rotor). A small pellet was observed at the bottom of the tube and occasionally a small white band was detected in the 25% layer. Most of the material was located at the 25/41% interface. This interface was collected, diluted in solution B, and centrifuged at 20,000 g for 20 min. The resulting pellet was saved for future study by resuspending in solution B and storing at either −20°C or 4°C.

Electron Microscopy

THIN SECTIONING: Pieces of the final pellet (see above) were fixed in 3% glutaraldehyde in 0.2 M sodium cacodylate buffer pH 7.4, for 30 min at room temperature. The solution was changed to a fixative containing 3% glutaraldehyde, 1% tannic acid, (1,600 mol wt; Sigma Chemical Co., St. Louis, MO), in 0.2 M sodium cacodylate (final pH 7.0) for 1 h at room temperature (55). After extensive washing with 0.1 M sodium cacodylate (pH 7.4), the pellet was postfixed in 2% osmium tetroxide in 0.1 M sodium cacodylate for 90 min. The pellets were washed in 0.2 M sodium acetate, pH 5.0, and block-stained overnight in 0.5% uranyl acetate in 0.2 M sodium acetate. The pellets were embedded in Epon, and sections having a gray interference color were cut with a diamond knife on an ultramicrotome (Reichert Model OMU2; American Optical, Southbridge, MA) The sections were deposited on carbon-coated grids and double-stained with uranyl acetate and lead citrate.

FREEZE-FRACTURE: Small samples (~0.1 μl) of a 3-4 mg/ml junction suspension were sandwiched between thin copper strips and plunged mechanically into liquid propane (−190°C) cooled with liquid nitrogen (12, 13). The resulting sample was ~10 μm in thickness, and the measured cooling rates were in excess of 10,000°C/s (0° to −100°C). The sandwiches were mounted in a hinged double-replica device adapted for use on a Balzers BA 360M (Balzers Co., Nashua, NH) freeze-fracture apparatus (13). A spring was activated to open the sandwiches and fracture the samples held at a pressure of 10^{-7} torr and a temperature of −160°C. The fractured samples were immediately replicated with platinum-carbon at 45° unidirectionally and carbon at 70° with rotation to provide a strong support film. The replicas were floated onto water, cleaned for 2-5 h in household bleach (Clorox), and mounted on uncoated 400-mesh grids.

NEGATIVE STAINING: A small aliquot of a junctional fraction (~1 mg/ml) was deposited on freshly prepared carbon-coated grids and washed with 1% uranyl acetate or sulfate (17). The grids were scanned at low magnification to select those junctions having a good stain deposition. The stained junctions were photographed at × 45,000 magnification, using minimum exposure techniques (56). The negatives were studied by optical diffraction to select the areas having sharp diffraction spots. Optical filtering was carried out according to the method of Erickson et al. (16). The microscopy was performed with a Philips EM 301 electron microscope.

X-ray Diffraction

X-ray diffraction patterns were recorded on Kodak No-Screen x-ray film loaded in a flat plate cassette camera as described previously (35). Copper K_α x-rays were obtained from a Jarrell-Ash stationary anode generator. Exposure times varied from 5 to 25 h with specimen-to-film distances set between 7 and 15 cm.

Unoriented fully hydrated preparations were made by centrifuging the junction suspension (~0.5-1 mg of protein) at 100,000 g for 1 h. The pellet was sealed in an x-ray capillary tube. Oriented specimens were produced by a method similar to the one used by Caspar et al. (9) in their study of isolated liver gap junctions but without chemical fixation. The lens junctions were centrifuged at 150,000 g for 2 h in a BEEM polyethylene capsule (Polysciences Inc., Warrington, PA) which was mounted on a Teflon adapter that fits at the bottom of a Beckman SW-41 rotor tube. The pellets were removed from the capsule and allowed to slowly dehydrate for various times at 4°C in a desiccator maintained at 93% humidity over a saturated solution of zinc sulfate. The specimen was then sealed in an x-ray capillary tube, along with a drop of saturated salt solution to maintain a constant humidity inside the tube. The capillary was mounted in the x-ray camera in a hollow brass block through which chilled water was circulated to keep the specimen at 4°C.

Other Methods

The protein concentration was determined by the method of Lowry et al. (31). The total phosphorus was determined by the method of Bartlett (1) and the cholesterol concentration was obtained as follows: various amounts of the sample as well as stock solutions of purified cholesterol (lot 2038; Applied Science, State College, PA) dissolved in chloroform/methanol 2/1 (vol/vol) were deposited on a silica gel G plate. The plate was developed in hexane:ethyl ether:acetic acid (70:25:5), vol/vol), dried under nitrogen, and sprayed with a solution containing 50% sulfuric acid in methanol. After drying, the plate was placed in an oven at 100°C. The cholesterol concentration was estimated by comparing the colors of the samples with those obtained from the standards.

SDS PAGE was done by the method of Weber and Osborn (51). Aliquots of the isolated junctions (10-65 μg protein) were solubilized in 3% SDS and 1% mercaptoethanol, heated at 60°C for ~5 min and immediately loaded at the top of a 7.5% polyacrylamide gel. Coomassie Blue-stained gels were scanned in a spectrophotometer at 570 nm (model 2400; Gilford Instrument Laboratories, Oberlin, OH).

RESULTS

Chemical Analysis

Our isolation procedure is similar to others (2, 5, 18, 24) but it differs in that it produces a pure fraction without using detergents or proteases. The protocol is simple and yields between 0.1-0.3 mg of pure junction protein/g of wet lens. Considering preparations of high purity, ours represents a significantly larger yield than reported previously (2, 5, 18).

Fig. 1 shows SDS PAGE optical density tracings of two different specimens. Fig. 1 *A* is comprised almost entirely of a band with an apparent molecular weight of 27,000 with two small additional peaks at 21,000 and 14,000. Fig. 1 *B* shows a scan of a gel from another preparation in which the 21,000 mol wt component is more pronounced but the 14,000 mol wt band is almost absent. These smaller peaks have been considered to represent an endogenous proteolytic derivative of the major 27,000 mol wt band (23, 47).

Our SDS polyacrylamide gels also showed that all the solubilized material entered the gel and that no additional bands were evident even upon overloading the gels. Similar gel patterns were obtained when the junctions were isolated in the presence of 10^{-4} M $CaCl_2$.

The protein/phospholipid/cholesterol ratio of the isolated junctions was approximately 1/0.6/0.2 wt/wt/wt in good agreement with previous studies (2, 5).

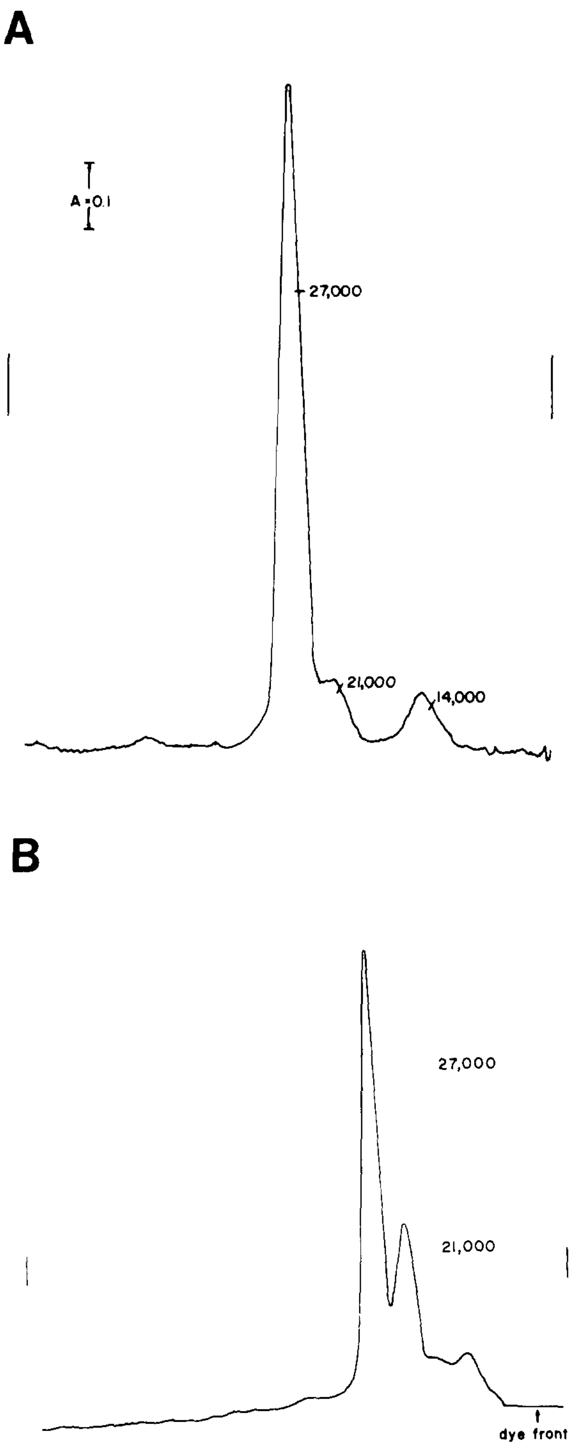

FIGURE 1 Optical density scans of 7.5% polyacrylamide gel patterns of two typical fractions of isolated lens junctions. The two lines indicate the top and bottom of the gels. The scan in Fig. 1 *A* corresponds to a gel to which 60 μg of solubilized protein was applied. Note that all the protein entered the gels.

Structural Studies

THIN SECTIONS: Figs. 2–4 show representative views of thin sections of the isolated junctions. Fig. 2*A* is a low-magnification view of the pellet showing the junctions either as a highly organized lamellar aggregate or as independent structures. Several of the aggregated structures were observed in each of the pellets. These two arrangements display junctions having slightly different structural features. The lamellar aggregate, which was probably formed during or subsequent to the isolation procedure, is about 6.5 μm long and 2 μm wide. It consists of concentrically arranged junctions that are separated by spaces 30–60 nm wide. The innermost junctions form continuous concentric layers with perimeters >10 μm, whereas the outermost ones appear as cisternae looping almost completely around the inner layers. The junctions in the aggregate undulate "in phase" with distances between crests of 0.3–0.5 μm. The more numerous independent junctions also have a wavy appearance (Fig. 2*A*, small arrows), but with somewhat smaller distances of 0.2 μm between crests. The independent junctions, in contrast to those seen in the aggregates, are often interrupted by small circular profiles ~0.1–0.3 μm in diameter as also shown in Fig. 3. Fig. 2*B* is a higher-magnification view of the area inside the dotted square in Fig. 2*A*. Here, each junction has a pentalamellar appearance (three dense strata separated by two light strata) having an overall thickness of 13–14 nm. In some places, the electron-dense strata of the pentalamellar structure appear asymmetric (i.e., each membrane having a different thickness). This apparent asymmetry (see Figs. 2–5) can be explained as a projection artifact due to curved surfaces in the plane of the junction. Fig. 2*B* and *C* show that the junctional membranes can separate and that the separations may occur anywhere along the length of the junction (Fig. 2*B*, arrow). However, the separations are most frequently observed at regions of high curvature (Fig. 2*C*, arrow).

Fig. 3 illustrates several structural details frequently observed in the independent junctions. Here, several junctions display their characteristic wavy appearance. Often the two membranes comprising the pentalamellar structure separate and enclose circular (*) or elongated (○) profiles which themselves form pentalamellar structures with each one of the original membranes. After encapsulating the profiles, the two junctional membranes reassume their original pentalamellar structure.

In Fig. 4, a straight junction is seen next to the more commonly observed undulating ones. This straight junction also has a pentalamellar structure but is much wider than the undulating junctions, as its overall thickness is 16–18 nm. This type was seen infrequently, suggesting that they are a small component of our isolated fraction. Also clearly seen in this figure (arrows) is a wavy junction whose membranes separate and form pentalamellar structures with an encapsulated profile. At the lower center of the field there is a junction whose membranes separate for ~0.4 μm before reassuming the normal pentalamellar appearance of the junction.

FREEZE-FRACTURE: Fig. 5 is a low-magnification view of a freeze-fracture replica of isolated lens junctions that are fractured obliquely, transversely, and frontally. The junctions fractured frontally display a corrugated surface having fracture faces at different levels. The distance between crests is ~0.5 μm, which correlates well with the undulations described in thin sections. Junctions fractured obliquely have the same characteristic undulations and frequently encapsulate circular profiles (Fig. 5, arrow).

Fig. 6 shows a replica that includes several junctions arranged somewhat like the junctions in Fig. 3. To the extreme left of the picture is a spherical body, enlarged in *D*, having patches displaying a square lattice casting shadows on a smooth surface. Fig. 6 *B*, *C*, *E*, and *F* are higher-magnification views of obliquely fractured junctions from the same micrograph. *B* and *F* are from regions outside the field in *A*, whereas *C* and *E* are the areas indicated by the arrows in *A*. For each of these

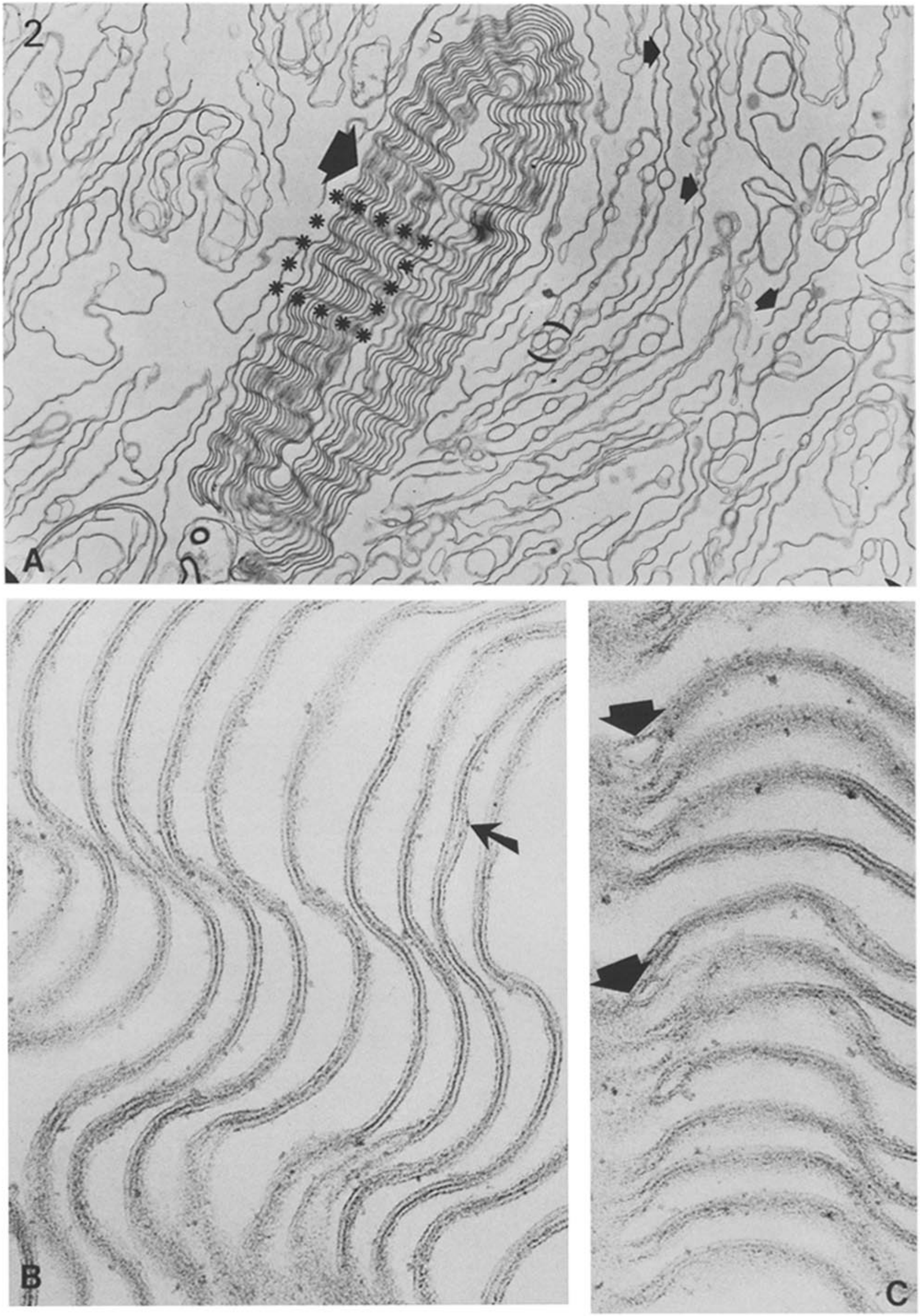
2
A
B
C

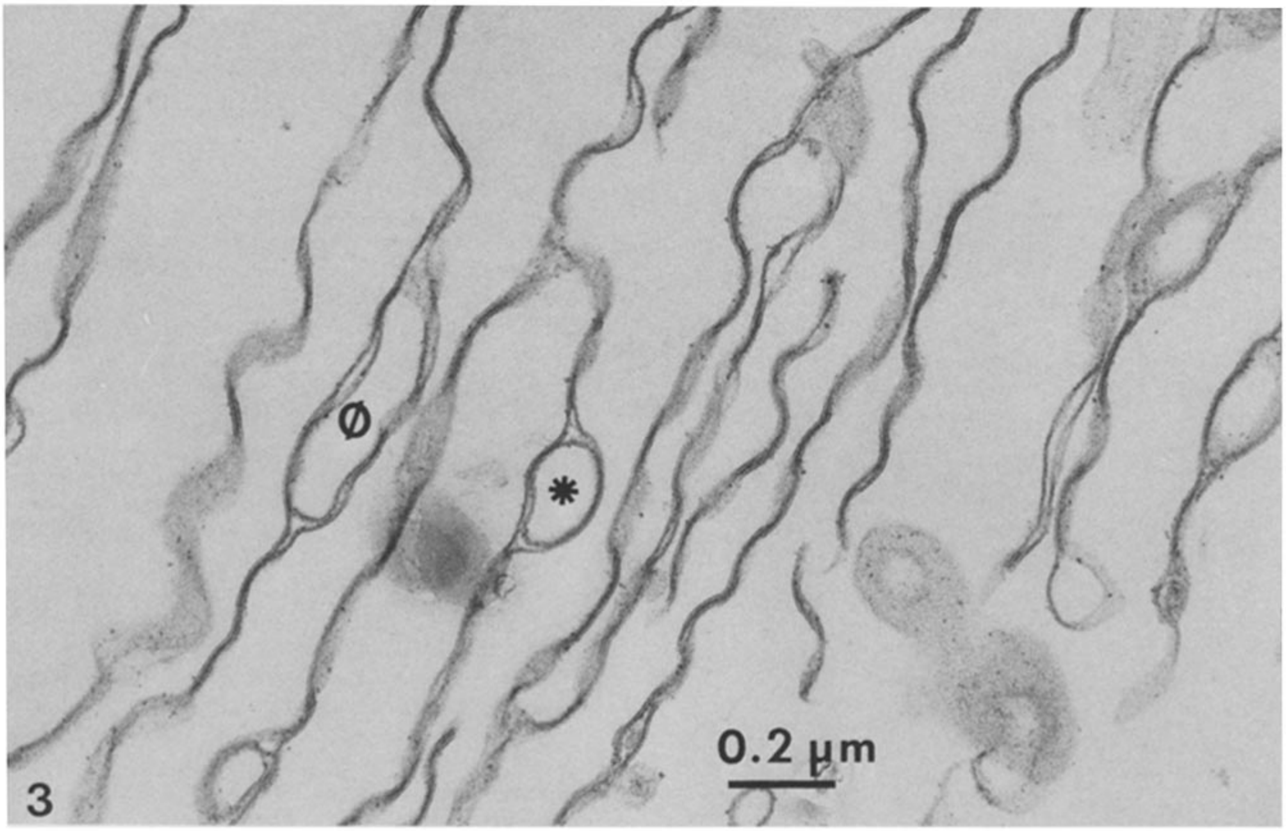

FIGURE 3 Thin-section electron micrograph of independent junctions. These junctions display the undulations seen in the aggregate in Fig. 2 and they frequently enclose circular (*) or elongated (Ø) profiles. × 80,000.

junctions, at least one of the membranes reveals repeating strips of metal alternating with shadows. It is apparent that most of these junctions are obliquely fractured, being tilted to the right or left, except for short segments of nearly vertical orientation. The repeating units are seen at the left edge of the junction in *E* and to the right edge of the one in *C*.

Fig. 7 shows an extensive region of an isolated junction. The nearly flat background surface labeled *2* is almost entirely covered with a square lattice. In the lattice there are prominent troughs that intersect at 90° and outline square patches. These patches show sets of orthogonal fine striations ~6–7 nm apart. The boundary between the square lattice and the surrounding smooth ice surface (lower right *inset*) appears jagged with many orthogonal edges. In some places whole pieces of the lattice are missing, leaving square or rectangular depressions. In such areas a smooth surface, labeled *3*, is seen at a level below the lattice surface. In other places smooth surfaces, labeled *1*, are seen raised above the surface of the lattice. The edges of these surfaces *1* are rounded. In a few places fragments of another component, labeled *4*, are seen lying on the rounded surfaces labeled *1* (upper left *inset*). This component is flat and raised above surface *1* by about the same distance that surface *2* lies above surface *3*. Surface *4* is smooth and has angular edges. In some places edges run in orthogonal directions.

Fig. 8*A* shows the striations in the fracture plane of surface *2* in Fig. 7 at a higher magnification. Fig. 8*B* is the optical transform of this micrograph. It consists of sharp reflections that index on a square lattice with a unit cell ~6.6 nm. Usually, only the first-order reflections are observed. Note the 90° angles between lines through the vertical and horizontal spots.

In Fig. 9, several junctions are seen fractured frontally. Large areas of ice are seen to the right top and below. As described above, we have identified four fracture surfaces numbered *1–4*. Note that the surface containing the square lattice and labeled *2* in the center of the field, is continuous with a region to its left that appears smooth but cratered by irregular pits. Note that on the right side of surface *2* the boundary between the edge of the surface and the surrounding ice is jagged and casts sharp shadows. Small areas of surface *4* are exposed at the borders of the lower ice mass. These surfaces are smooth and have jagged edges.

The features of the unusual fracture patterns described for Figs. 6–9 can be seen in stereo in Fig. 10. A twist of the fracture plane of the junctional membrane on the right (middle arrow) reveals that the various textures observed are not entirely dependent on the shadow angle. Fractures of both junctional membranes are clearly observed. A number of junctions fractured frontally are shown to the left. One obliquely fractured

FIGURE 2 Thin-section electron micrograph of the isolated junctions. *A* is a low-magnification view of the pellet showing a prominent lamellar aggregate and many independent junctions that frequently enclose circular profiles (parentheses). The region inside the square is shown at higher magnification in *B*. Each junction has a pentalamellar structure that, at places (arrow), separates into two membranes. *C* is the region indicated by the large arrow in *A*. Note that the separations are aligned. (*A*) × 17,000. (*B* and *C*) × 180,000.

junction is seen to the right bordered on both sides by ice. The membrane to the right very clearly displays surface *2* with its lattice pattern. In the center of the figure at the large arrow, this membrane is seen in nearly edge-on view. The lattice shows up here as transverse bands of metal ~7 nm long and spaced ~7 nm apart. To the lower left (at the arrow) the two membranes are separated and a layer of ice is seen between them.

An important result from the freeze-fracture study of these isolated lens junctions containing crystalline arrays is that conventional intramembrane particles are not present on any of the exposed fracture surfaces.

NEGATIVE STAINING: Fig. 11*A* is a representative view of a region of an isolated junction negatively stained with uranyl sulfate (17). The arrow points to an edge-on view of the structure showing that it contains two membranes. The flat junctional area exhibits low contrast but clearly shows, particularly when viewed obliquely, a crystalline lattice consisting of orthogonal rows of particles. Fig. 11*B* is a region from another junction that also shows the array of units. Its optical transform (Fig. 11*C*) consists of weak but sharp reflections that index on a square lattice having a unit cell of ~6.5 nm. These reflections are similar to those seen in the optical transform of the freeze-fracture replicas (Fig. 8*B*) but of far lower intensity. The low-contrast periodic features detected in the image can be emphasized by optical filtering (16). Fig. 11*D* shows a low-resolution filtered image having electron-lucent regions (presumed to be part of the protein) and electron-dense pools of stain located at the corners. The low contrast observed in the negatively stained images and the low intensity of the reflections in the optical transforms can be explained by assuming that only small portions of the protein oligomers are contained in the stained areas.

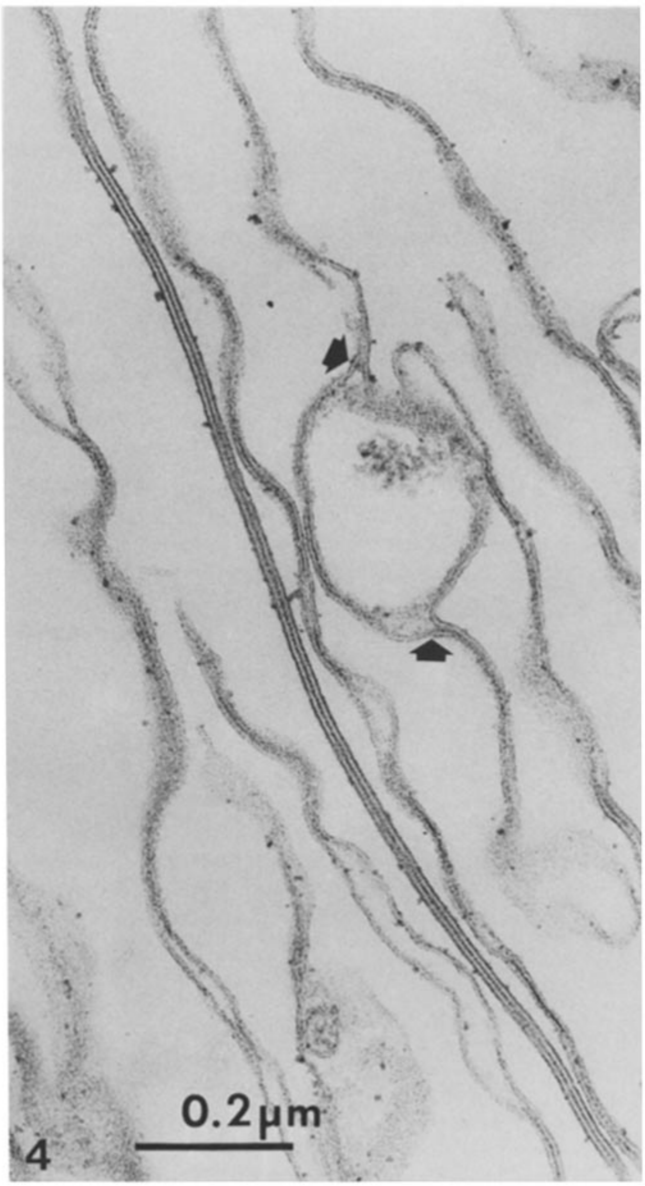

FIGURE 4 Junctions having a straight profile are sometimes observed in the pellets. They have a greater overall thickness than the undulating junctions. The arrows point to regions where the membranes of an undulating junction separate to enclose a circular profile. Note the extensive separation between membranes in the junction at the lower right side of the figure and that the individual membranes are also undulating. × 110,000.

X-RAY DIFFRACTION: X-ray diffraction patterns from unoriented, fully hydrated, isolated junctional pellets contain weak but sharp rings at 6.6 and 3.3 nm along with a diffuse ring at 0.45 nm. Additional information was obtained from junctions that were oriented by a slow, controlled dehydration procedure. Fig. 12*A* shows a wide-angle diffraction pattern from a specimen that was equilibrated at 93% relative humidity for 12 h. The pellet was mounted so that the long axis of the centrifuge tube was oriented in the vertical direction relative to the x-ray film. Thus, the broad diffraction bands on the vertical axis (meridian) arise from the partial stacking of the junctions. The horizontal axis (equator) of the x-ray film shows several reflections arising from repeating units located in the plane of the oriented junctions. The broad 0.45-nm reflection (large arrow), which arises from the hydrocarbon chains, is partially oriented, being more intense at the equator. The small arrow points to a reflection at 3.3 nm. Fig. 12*B* is a more lightly exposed film from the same pellet, magnified so that it shows the scattering located close to the beam stop. In Fig. 12*B*, arrows point to sharp equatorial reflections at 6.6 and 3.3 nm. On the meridian, in *A* and *B* there is a partially resolved broad band at ~14 nm (seen better in *D*) with other broad bands at 7.7, 4.2, 3.0, and 1.65 nm; while the sharp reflections on the equator are located at 6.6, 3.3, 1.84, 1.57, 1.30, 1.11, and 0.95 nm. These equatorial reflections index on a square lattice of 6.6 nm. When the specimens were equilibrated for 24 h or longer at 93% relative humidity, better orientation was obtained (Fig. 12 *C* and *D*). The patterns show the same sharp reflections arising from the units repeating with a lattice constant of 6.6 nm. With equilibration times >48 h, the inner meridional reflections at 14 and 7.7 nm diminished in intensity and additional sharp reflections at 3.4 and 1.7 nm appeared. These additional reflections are consistent with cholesterol forming a separate phase (29).

A key result of these experiments is that sharp reflections at 6.6 and 3.3 nm, arising from units located in the plane of the junctions, are observed in all patterns from fully and partially hydrated pellets. Also, no other equatorial reflections are observed in the range of 3.0 to 15 nm. These same patterns were found in junctions bathed in 10^{-4} M EDTA (without calcium present) at pH 8.0.

DISCUSSION

General Structural Features of Isolated Crystalline Lens Junctions

The major difference between our isolation procedure and those described by other investigators (2, 5, 18, 24) is that it

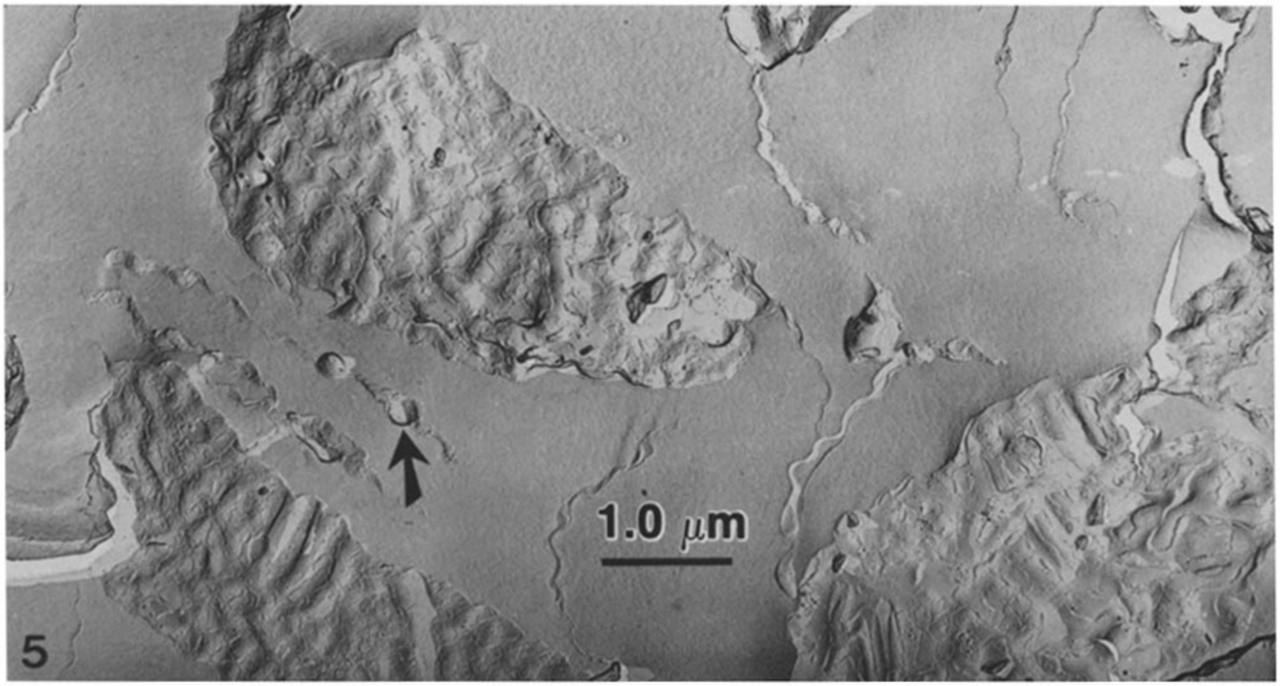

FIGURE 5 Freeze-fracture replica of the isolated lens junctions at low magnification. Note that the undulating surfaces are seen in both oblique and transverse fractures. × 17,000.

produces a pure fraction in high yield without using detergents or proteases. The major protein of the junctions is a polypeptide having an apparent molecular weight of 27,000. The Coomassie-Blue gel-staining patterns of our fractions are in good agreement with those obtained by other preparative techniques that use detergents (18). The ratio of 1.0/0.6/0.2 (wt/wt/wt) of protein/phospholipid/cholesterol is also in good agreement with values previously reported (2, 5) and show that there is a high protein/lipid ratio in the fractions. If we assume molecular weights of 27,000, 800, and 386 for the protein, phospholipid, and cholesterol, respectively, then the above ratio corresponds to a molar ratio of 20 phospholipid and 15 cholesterol molecules for each protein monomer.

The isolated fraction is comprised of junctions, i.e., two plasma membranes intimately apposed. This result is demonstrated by electron microscopy using thin-sectioning (Fig. 4), negative-staining (Fig. 11), and freeze-fracture techniques (Figs. 6 and 10). This conclusion is also supported by low-angle x-ray diffraction analysis of junctional pellets. The x-ray diffraction patterns show broad meridional bands at 14, 7.7, 4.2, 3.0, and 1.65 nm consistent with the transform of a membrane pair as in liver gap junctions (33) but not of a single membrane (21). The x-ray pattern also shows the 0.45-nm broad reflection characteristic of lipids in the liquid crystalline phase (32, 52).

Both the negative-staining and freeze-fracture techniques reveal surfaces composed of units arranged in a square lattice with a fundamental spacing of 6.6 nm (Figs. 7 and 11). In this study, this is the only crystalline organization observed with either of these techniques. However, most microscope studies present sampling problems that make the relationship between the observed images and the average structure of the sample difficult to assess. Consequently, we have used x-ray diffraction analysis to obtain the average spacings of the entire sample (1 mg of protein or $\sim 2.2 \times 10^{16}$ protein molecules). The only x-ray reflections recorded from the plane of the junction (in the range from 15 to 3.0 nm) are the 6.6- and 3.3-nm reflections. This is strong evidence that the square lattice is the predominant crystalline form in the isolated junctions. We note that reflections from hexagonal gap junctions, which have a fundamental spacing of ~8.5 nm when isolated from liver (9), have not been observed in the patterns obtained from our isolated lens junctions. However, we have occasionally observed straight profiles in sections of pellets of the fraction that are thicker (16–18 nm) and which appear to be gap junctions (Fig. 4). This is consistent with the observations of others who have recognized gap junctions in the lens (2, 3, 19, 26, 38, 39, 41, 42). A major difference in our results is that, while others have reported the gap junction to be the dominant junction in the lens (2, 3, 18, 24), we find the gap junction to be a minor component in comparison with the square junction (see Figs. 2–4).

We interpret the square lattice to be a two-dimensional array of protein units located in the plane of each junctional membrane. The freeze-fracture images (Fig. 10) indicate that the units span the entire thickness of the bilayer. We do not have data of resolution high enough to say with certainty that the square lattice is tetragonal (i.e. has fourfold symmetry). The lattice could be classified as p1, p2, or p4. However, if one considers the molecular weight of the protein, the protein/lipid mole ratios, and the dimensions of the unit cell, it seems very likely that there are four protein molecules per unit cell.[1] This

[1] The volume of the unit cell (283–305 nm^3) in each membrane is calculated by multiplying the area of the square $(6.6\ nm)^2$ by one half the thickness of the junction (6.5–7.0 nm). The volume of a 27,000 mol wt protein is ~35 nm^3 (48). The volume of each lipid molecule (1.0 nm^3) can be estimated by multiplying the partial molar area (0.43 nm^2) (29) by one half the thickness of a bilayer having this composition (2.4 nm) (29). Thus, a volume of 70 nm^3 is obtained for each protein and its complement of 35 lipids (see Chemical Analysis above). Finally, the volume of each unit cell divided by this protein-lipid volume of 70 nm^3 gives a value of 4.0–4.4 proteins per unit cell. We note that this calculation makes no assumptions about the molecular arrangement of protein and lipid in the membrane.

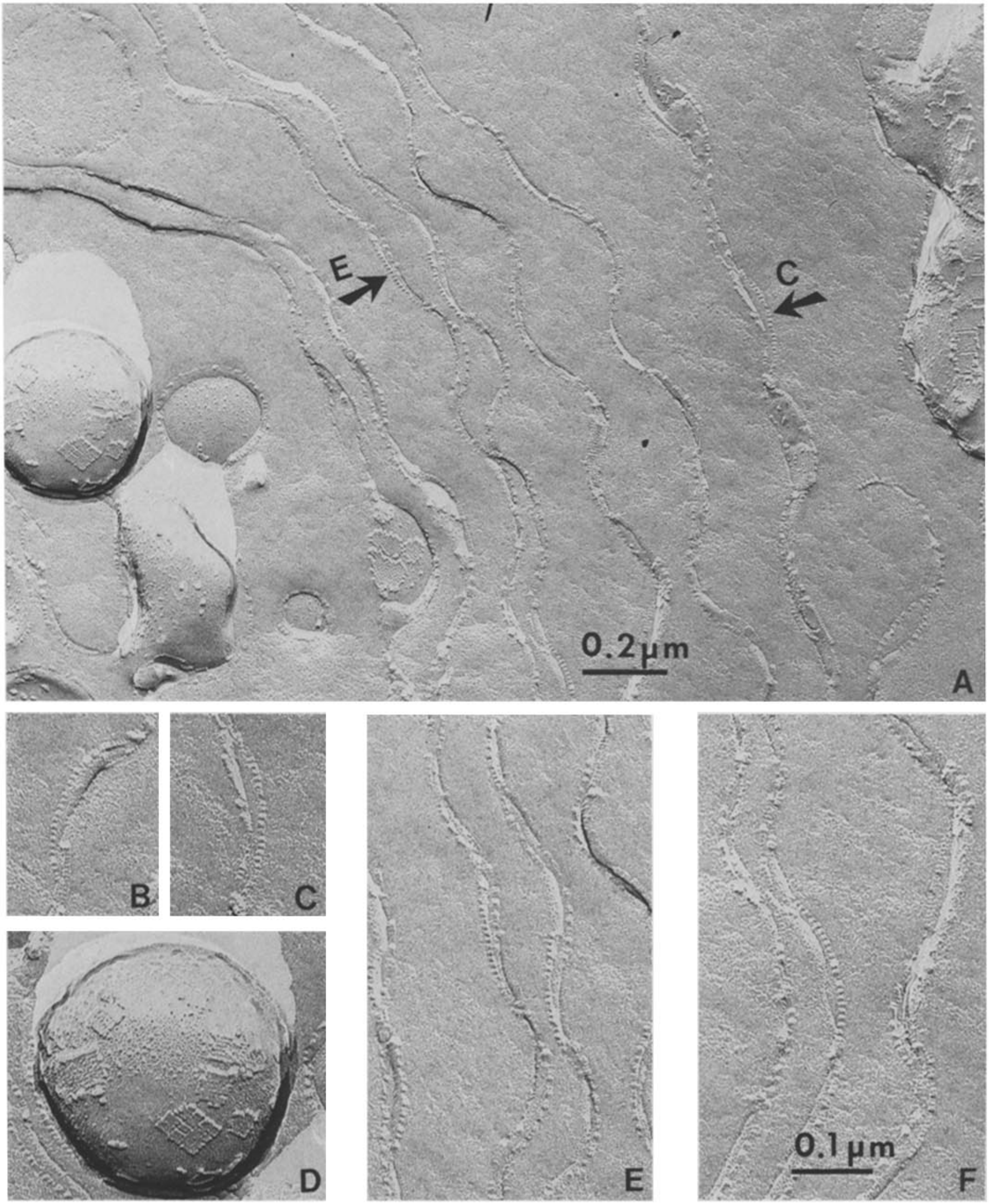

FIGURE 6 (*A*) Freeze-fracture replica of a loose arrangement of isolated junctions. In the center of the field seven junctions are seen obliquely fractured. The two segments marked by arrows labeled *C* and *E* are enlarged below in panels *C* and *E*, respectively. Two other segments from the same micrograph but out of the field are enlarged in (*B*) and (*F*). The spherical area to the left is enlarged in *D*. (*A*) × 80,000. (*B–F*) × 150,000.

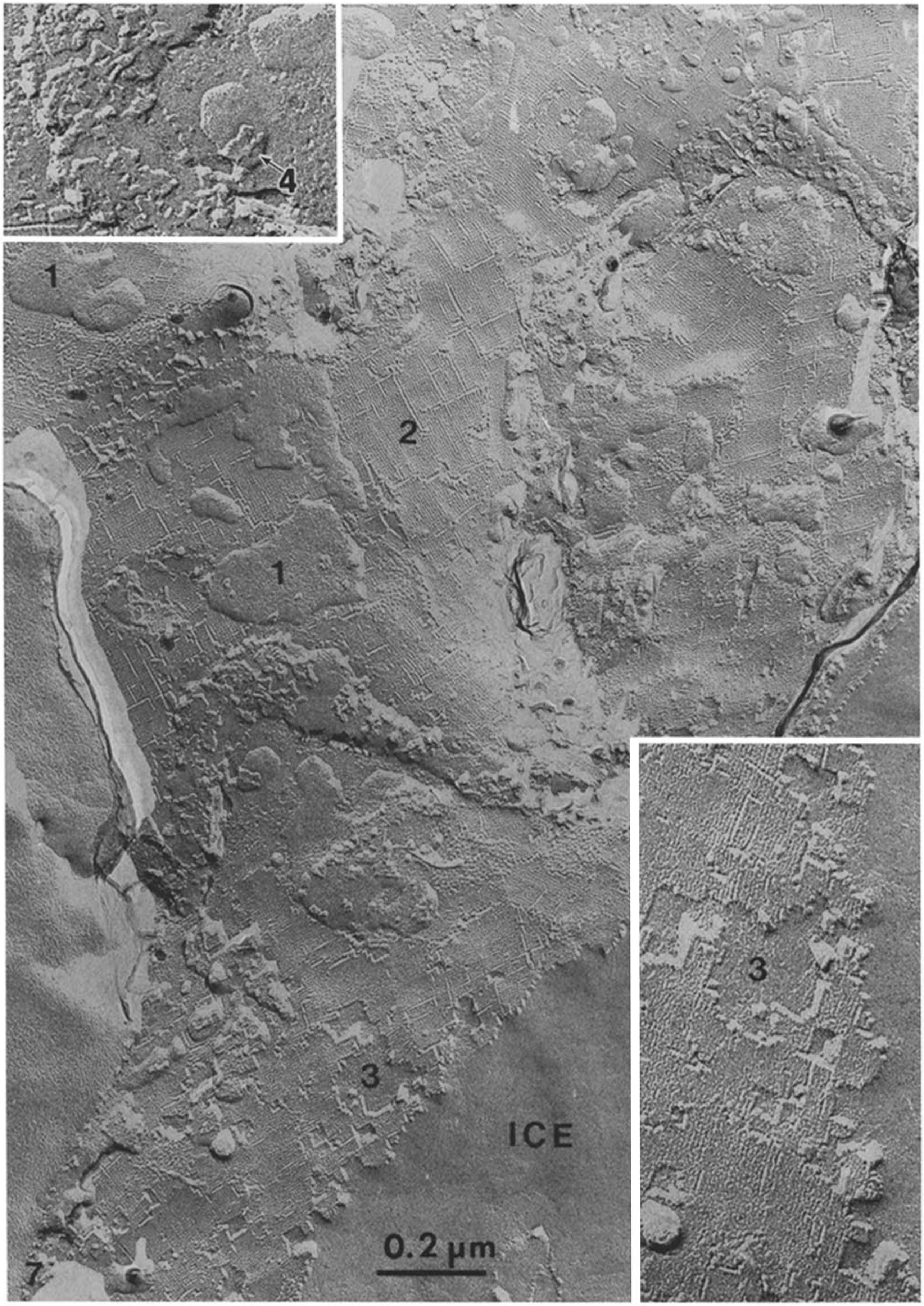

FIGURE 7 An extensive fracture face composed almost exclusively of square lattices. This junction was in a solution containing Tris buffer (pH 8.0) and 1.6×10^{-8} M calcium concentration. Under these ionic conditions, the square array was the only regular packing observed. Four fracture surfaces designated *1–4* are shown. See text for further details. × 100,000. The lower *inset* shows the jagged edges of the fractured junctions at the ice boundary. Lower *inset*, × 180,000. The upper *inset* shows fragments of a crystalline membrane resting on surface *1*. The upper surface of the fragments is surface *4*. × 180,000.

makes the p4 lattice an attractive possibility and means that the protein in the structural unit is probably a tetramer.

Correlation with Previous Structural Studies

Previous studies by thin sectioning (10, 11, 27, 30, 43, 50, 53) and scanning electron microscopy (15, 27, 34) of the whole lens have shown extensive interdigitations covering much of the surface of lens fiber cells in the deep cortex and nucleus. Dickson and Crock (15) referred to these as "tongue-and-groove" junctions. Their general appearance including the amplitude and period is similar to that of our isolated undulating junctions. Therefore, it seems likely that most of our isolated fraction consists of tongue-and-groove junctions of intact lens fibers. We have found no indication of cytoskeletal elements in the isolated junctions either by electron microscopy or in SDS gels. This suggests that the characteristic shape of the tongue-and-groove undulations can be produced by properties of the intrinsic membrane components. We note that, in the sections of the isolated junctions in Figs. 2–4, adjacent

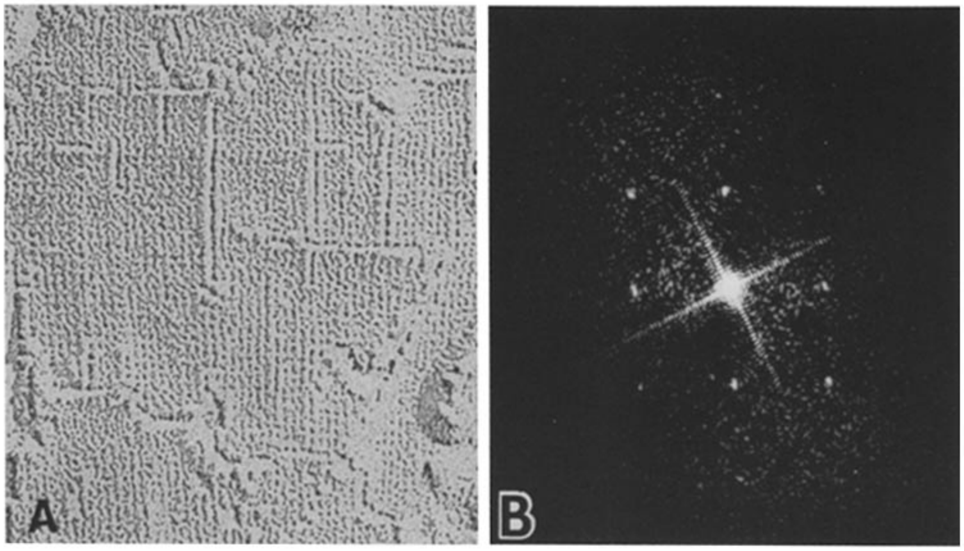

FIGURE 8 Higher-magnification view of a region in Fig. 7 (*A*). The fractured surface contains pronounced grooves and fine striations. × 230,000. (*B*) The optical transform shows only the first-order reflections that index on a square lattice having a lattice constant of 6.5 nm.

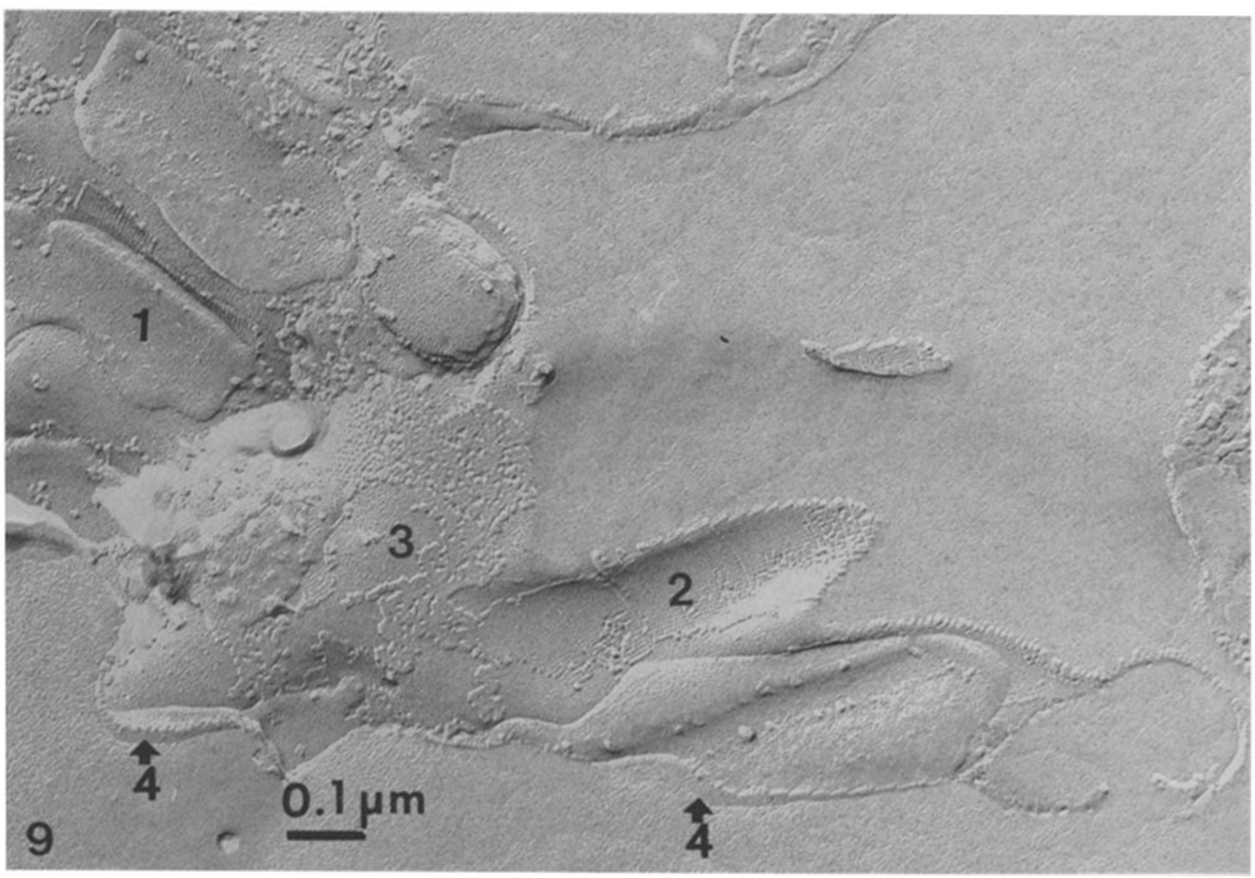

FIGURE 9 Oblique fractures through several junctions showing four fracture surfaces (*1–4*). Note that surface *2* is continuous with a smooth surface (to the left) which does not show the lattice and with a cratered surface (upper left). These features are not characteristic of typical hydrophobic fracture surfaces. × 105,000.

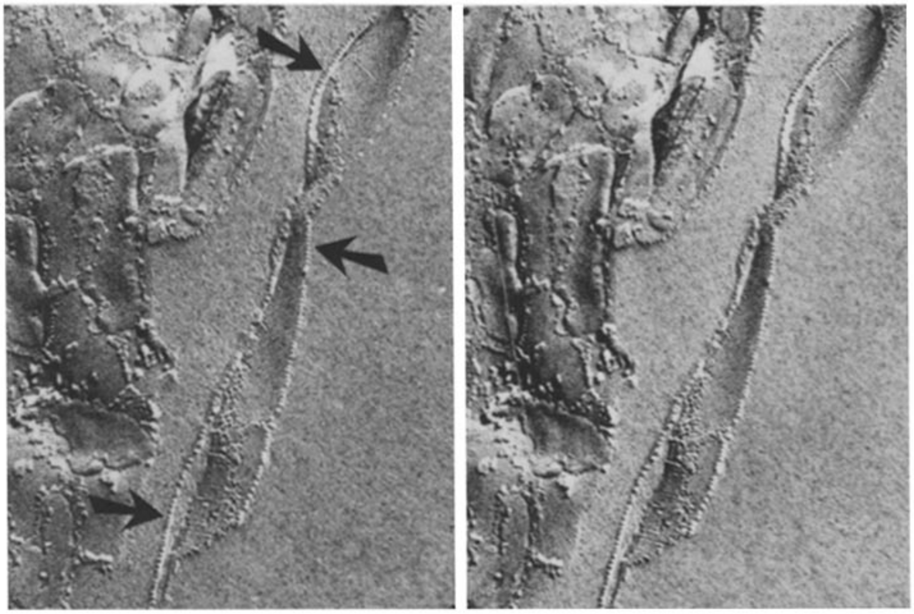

FIGURE 10 Stereo pair showing the different fracture surfaces described in this study. Note that the usual intramembrane particles are absent and that fractures at the edges of membranes clearly show structural units spanning the membranes (arrows). × 75,000.

junctions undulate in phase thereby maximizing attractive van der Waals interactions (37).

The square crystalline array, though not always referred to as "square," has previously been observed in freeze-fracture replicas by several workers in intact lenses or lens fragments (3, 19, 25; also see Fig. 4 in reference 38). In agreement with observations in these previous reports, our preliminary studies (14) of fragments from rat lens cortex also show patches of square lattice which appear identical to those of our isolated junctions. Square arrays also have been observed by a number of workers in isolated fractions of varying purity (3, 18, 25, 39, 41, 42). However, they were not characterized nor recognized as constructed from the major protein of the lens junctions. In fact, they were interpreted variously as a contamination from other components of the lens (18), the result of mild proteolysis (25), or as another crystalline state of the gap junction protein (41, 42).

An important difference between our findings and those of previous studies is that we observed more extensive square lattices (Fig. 7) without using proteases or calcium treatments. For example, Kistler and Bullivant (25) observed square arrays in single membranes after mild trypsinization. They correlated the square array with the presence of a 16,000 mol wt SDS band, which they interpreted to be a cleavage product arising from treatment with trypsin. Our junctions, isolated under similar ionic conditions and pH, but without trypsinization, were devoid of a 16,000 mol wt band but do show bands at 21,000 and 14,000 mol wt. The presence of these minor components cannot explain the extensive crystalline lattice demonstrated in our electron-microscopy (Fig. 7) and x-ray diffraction studies (Fig. 12). Moreover, we have observed the square array in freeze-fracture replicas of junctions both when the apposing membranes are in close contact and when there is a wide fluid space between them (Fig. 10). Peracchia and Peracchia (41, 42) have observed in crude membrane homogenates hexagonal, tetragonal, and rhomboidal lattices as well as the random arrays usually identified as gap junctions. They consider these crystalline lattices to result from transformation of the random arrays by treatment with calcium or by low pH treatment. However, we have consistently observed the square arrays by three techniques at pH 8 in sufficient EDTA buffer to reduce the $[Ca^{++}]$ to 10^{-8} M. One possible explanation that cannot be ruled out for the difference between their results and ours is that some step in our isolation procedure causes the subunits to crystallize and remain so even at low calcium concentration and high pH.

Several investigators (3, 41, 42) have proposed that square lens junctions and hexagonal liver gap junctions may represent two different crystalline states of the same protein. However, this interpretation seems unlikely if we take into account the differences reported in the amino acid compositions (6, 19), and their tryptic digestion maps (22, 23) and partial sequences (36). Also, these junctions are antigenically distinct (57), they crystallize in different lattices, and they differ in other ways as well (see Table I). It thus seems reasonable to conclude that the square junctions and the gap junctions contain distinct proteins and may belong to two different classes of intercellular contacts.

Square arrays with dimensions strikingly close to the ones described here in lens junctions have been observed in several types of cell membranes such as in the epidermis of larval salamandra (46) and astrocytes (27). These do not, however, occur in extended arrays as in the lens, their fracturing characteristics are different, and they often occur in nonjunctional membranes.

Freeze-fracture Patterns

The most striking feature of the fractured surfaces is the presence of extended square arrays (surface *2* in Figs. 7 and 9). The appearance and dimensions of the lattice are totally consistent with the thin-section, negative-stain, and x-ray diffraction data. These results together with the high protein content of the fraction indicate that a crystalline arrangement of protein exists in the plane of the membranes. Regions where the crystalline arrays (see Fig. 7, lower *inset*) are fragmented and where fractures expose the edges of the lattices (see Figs. 6 and 10) suggest that the structural units span the entire thickness of the membranes. These key features of the fracture patterns are not dependent on knowing the location of the fracture plane within the membrane pair.

On the other hand, a precise localization of the plane of

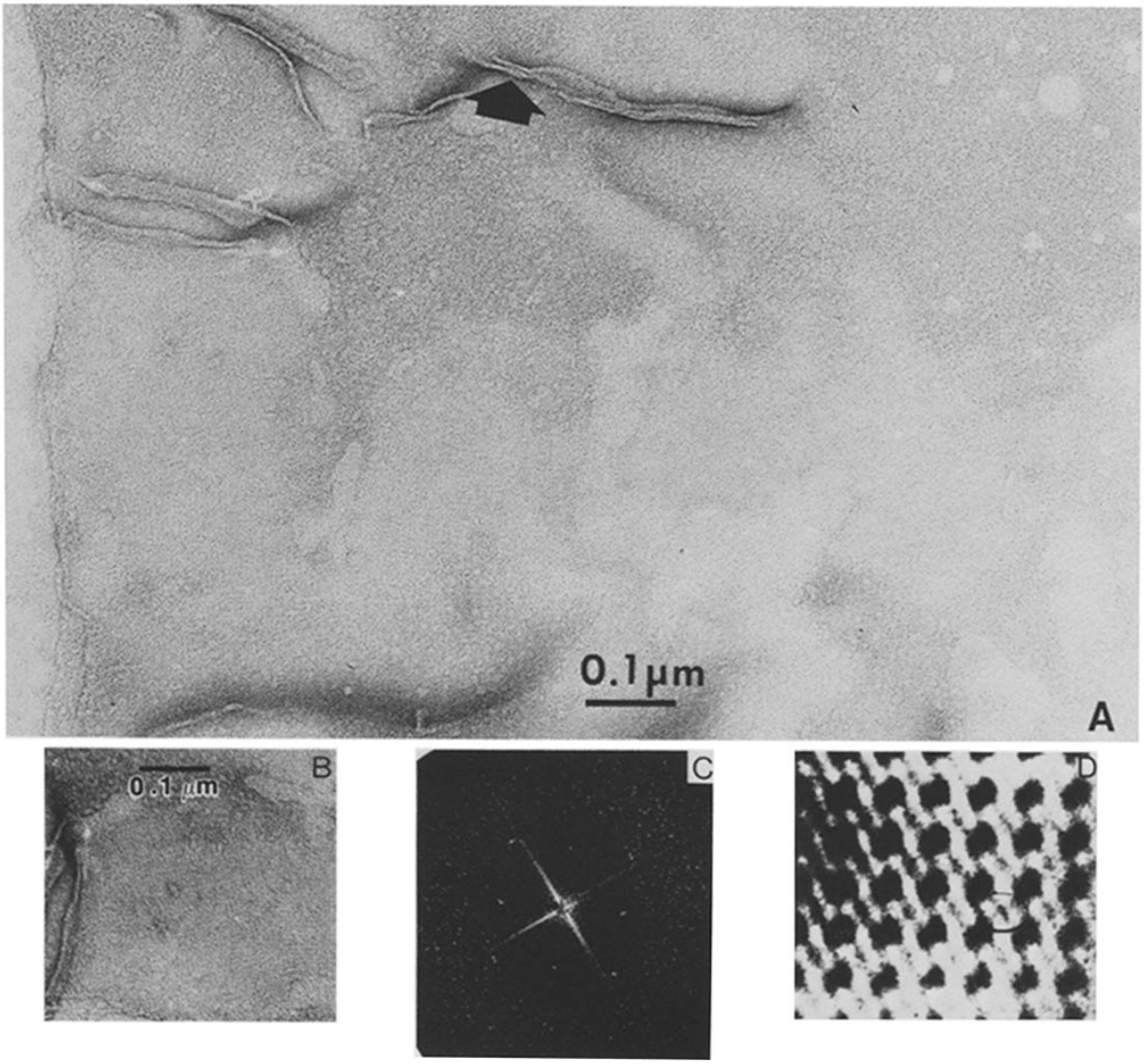

FIGURE 11 Isolated junction negatively stained with uranyl sulfate. *A* is a low-magnification view of a flat junction. An edge-on view shows that these structures are junctions (arrow). *B* is a small region of another junction whose optical transform is shown in *C*. The filtered image (*D*) shows the presence of a square lattice; black circle delineates one unit. (*A* and *B*) × 135,000. (*D*) × 1,100,000.

fracture is essential in understanding how the observed surfaces develop and how they relate to the fractures reported in other studies (2, 3, 7, 18, 24, 25, 38, 41, 42). Interpretation of the exposed surfaces in terms of fractures along membrane hydrophobic interiors (exposing P-fracture face (PF) and E-fracture face (EF) surfaces) cannot fully explain the fracture patterns. None of the four exposed surfaces display typical intramembrane particles or pits and none of the surfaces are related by EF-to-PF fracture steps such as those reported in previous studies of lens fiber cells. Even the large particles seen on surface *1* (Fig. 7, upper *inset*) can be interpreted as fragments of crystalline membranes rather than intramembrane particles.

An alternative interpretation of this unusual fracture pattern is that the fracture proceeds along membrane surfaces. For example, surface *2* (see Figs. 7 and 10), which displays the square array, is separated from the ice by a step of about the thickness of one crystalline membrane; this suggests that surface *2* could be an external (or ES) fracture surface. Surface *1* occurs within the space between junctional membranes (see Figs. 7 and 10) and probably corresponds to ice covering surface *2* at locations where the junctional membranes separate (Fig. 2 *B*, arrow, and Fig. 10). Surface *4* (see Fig. 7, upper *inset*, and Fig. 9), which is rarely exposed in our replicas, can be interpreted as the protoplasmic (or PS) surface. Surface *3* (Fig. 7), which is more commonly seen, seems to be complementary to surface *4* and exposes the ice surrounding the junction. Surfaces *3* and *4* are both smooth and do not show the square pattern. Although this assignment of fracture surfaces is unconventional, it does satisfactorily explain the unique appearance of the four fracture surfaces and their interrelationships seen in the replicas.

Conclusions

We have presented chemical and structural data indicating that the isolated lens junction may represent a new class of

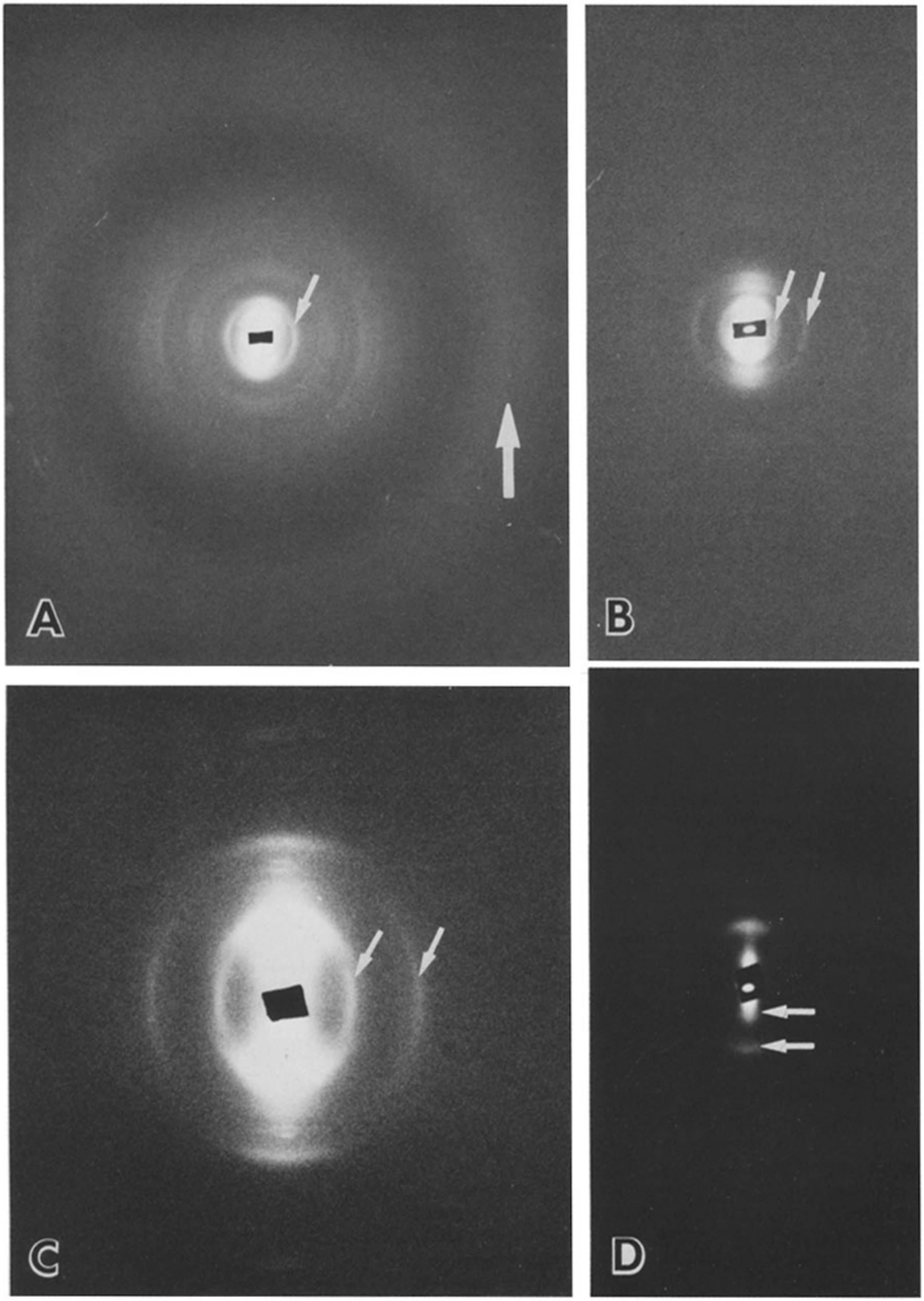

FIGURE 12 Wide-angle (*A* and *B*) and low-angle (*C* and *D*) diffraction patterns of oriented, partially hydrated lens fiber junctions. Each diffraction pattern is mounted so that the axis of the centrifuge tube would be in the vertical direction. *A* shows a broad diffuse band centered at 0.45 nm (large arrow). The sharp reflections along the horizontal axis arise from the lattice in the place of the junction. The small arrow points to the reflection at 3.3 nm. The scattering on the vertical axis (arising from the partial stacking of junctions) consists of several broad bands, with the innermost bands being unresolved in this wide-angle pattern. *B* is the second film of a similar pattern, printed at higher magnification to show the sharp in-plane reflections at 6.6 nm and 3.3 nm (arrows). The vertical axis of this pattern shows broad bands centered at 7.7, 4.2, and 3.0 nm. *C* is a low-angle pattern of a specimen which had been equilibrated at 93% relative humidity for 48 h. The sharp in-plane reflections at 6.6 and 3.3 nm are marked with small arrows. *D* shows a pattern with lower exposure time to demonstrate the broad bands located close to the beam-stop and centered at about 14 and 7.7 nm (arrows).

TABLE I
A Comparison of Isolated Lens Junctions and Liver Gap Junctions

	Lens	Liver	References	
			Lens	Liver
Structure				
Overall thickness	13.5 nm	16.0 nm	This work	9, 54, 55
Packing of oligomers	Square	Hexagonal	This work	20, 56
Unit cell	6.6 nm	8.5 nm	This work	56
Surface topology	Undulating	Flat	This work	54, 55
Chemical				
Subunit mol wt	27,000	26,000	This work, 7, 18	20
Amino acid composition	Different		7	20
Phospholipid/cholesterol M/M	3:2	1:1	This work, 7	20
Immunological properties	No cross-reactivity			22

intercellular contact. Although there are some similarities between the lens junctions and the liver gap junctions, the differences between them are so significant that they cannot be considered to be the same. Although the function of this lens junctional complex remains to be determined, it is not necessarily involved in intercellular communication. Perhaps it is involved in other interactions between the cells necessary to maintain lens transparency such as minimizing extracellular space or controlling homeostasis in the fiber cells.

The authors wish to thank Drs. W. Freytag, J. Corless, and W. Longley for helpful discussions. We are grateful to Ms. Ann Graham and Ms. Patrice LeClerc for their excellent clerical assistance.

This research was supported in part by the following National Institutes of Health grants: GM 07403, GM 27278, GM/AM 28224, and GM 27914.

Received for publication 8 June 1981, and in revised form 9 November 1981.

REFERENCES

1. Bartlett, G. R. 1958. Phosphorous assay in column chromotography. *J. Biol. Chem.* 244: 4406–4412.
2. Benedetti, E. L., I. Dunia, C. J. Bentzel, A. J. M. Vermorken, M. Kibbelaar, and H. Bloemendal. 1976. A portrait of plasma membrane specializations in eye lens epithelium fibers. *Biochim. Biophys. Acta.* 457:353–384.
3. Benedetti, E. L., I. Dunia, F. C. S. Ramaekers, and M. A. Kibbelaar. 1981. Lenticular plasma membranes and cytoskeleton. *In* Molecular and Cellular Biology of the Eye Lens. H. Bloemendal, editor. 137–188.
4. Bok, D., and J. Horwitz. 1980. Immunocytochemical localization of the main intrinsic membrane protein in lens fiber membranes. *J. Cell Biol* 87(2, Pt. 2):1517*a* (Abstr.).
5. Broekhuyse, R. M., and E. D. Kuhlmann. 1978. Lens membranes. IV. Preparative isolation and characterization of membranes and various membrane proteins from calf lens. *Exp. Eye Res.* 26:305–320.
6. Broekhuyse, R. M., and E. D. Kuhlmann. 1980. Lens membranes. XI. Some properties of human main intrinsic protein (MIP) and its enzymatic conversion into a 27,000 dalton polypeptide. *Exp. Eye Res.* 30:305–310.
7. Broekhuyse, R. M., E. D. Kuhlmann, J. Bijvelt, A. J. Verkleij, and P. H. J. T. Vevergaert. 1978. Lens membranes. III. Freeze-fracture morphology and composition of bovine lens fiber membranes in relation to aging. *Exp. Eye Res.* 26:147–156.
8. Broekhuyse, R. M., E. D. Kuhlmann, and H. J. Winkens. 1979. Lens membranes. VII. MIP is an immunologically specific component of lens fiber membranes and is identical with 26K band protein. *Exp. Eye Res.* 29:303–313.
9. Caspar, D. L. D., D. A. Goodenough, L. Makowski, and W. C. Phillips. 1977. Gap junction structures. I. Correlated electron microscopy and x-ray diffraction. *J. Cell Biol.* 74:605–628.
10. Cohen, A. 1958. Electron microscopic observations on the lens of the neonatal albine mouse. *Am. J. Anat.* 103:219–245.
11. Cohen, A. 1965. The electron microscopy of the normal human lens. *Invest. Ophthalmol.* 4:433–446.
12. Costello, M. J. 1980. Ultra rapid freezing of thin biological samples. *Scanning Electron Microsc.* II:361–370.
13. Costello, M. J., and J. M. Corless. 1978. The direct measurement of temperature changes within freeze-fracture specimen during rapid quenching in liquid coolants. *J. Microsc.* (*Oxf.*). 112:17–37.
14. Costello, M. J., Ting-Beall, H. P., and J. D. Robertson. 1982. Fractures along the hydrophilic surfaces of mammalian lens fiber cell membranes. *Biophys. J.* 37(2, Pt. 2): 276*a* (Abstr.).
15. Dickson, D. H., and G. W. Crock. 1972. Interlocking patterns on primate lens fibers. *Invest. Ophthalmol.* 11:809–815.
16. Erickson, H. P., W. A. Voter, and k. Leonard. 1978. Image reconstruction in electron microscopy: Enhancement of periodic structure by optical filtering. *Methods Enzymol.* 49(Pt. G):39–63.
17. Estis, L. F., R. H. Haschemeyer, and J. S. Wall. 1981. Uranyl sulfate; a new negative stain for electron microscopy. *J. Microsc.* (*Oxf.*). 124:313–318
18. Goodenough, D. A. 1979. Lens gap junctions: a structural hypothesis for nonregulated low-resistance intercellular pathways. *Invest. Ophthalmol. Visual Sci.* 18:1104–1122.
19. Goodenough, D. A., J. S. B. Dick II, and J. E. Lyons. 1980. Lens metabolic cooperation: a study of mouse lens transport and permeability visualized with freeze-substitution autoradiography and electron microscopy. *J. Cell Biol.* 86:576–589.
20. Henderson, D., H. Eibl, and K. Weber. 1979. Structure and biochemistry of hepatic gap junctions. *J. Mol. Biol.* 132:193–218.
21. Henderson, R. 1975. The structure of the purple membrane from *Halobacterium halobium*: analysis of the x-ray diffraction pattern. *J. Mol. Biol.* 93:123–138.
22. Hertzberg, E. L. 1980. Biochemical and immunological approaches to the study of gap junctional communication. *In Vitro* (*Rockville*). 16:1057–1067.
23. Horwitz, J., and M. M. Wong. 1980. Peptide mapping by limited proteolysis in sodium dodecylsulphate of the main intrinsic polypeptides isolated from human and bovine lens plasma membranes. *Biochim. Biophys. Acta.* 622:134–143.
24. Kistler, J., and S. Bullivant. 1980. The connexon order in isolated lens gap junctions. *J. Ultrastruct. Res.* 72:27–38.
25. Kistler, J., and S. Bullivant. 1980. Lens gap junctions and orthogonal arrays are unrelated. *FEBS* (*Fed. Eur. Biochem. Soc.*) *Lett.* 111:73–78.
26. Kuszak, T., H. Maisel, and C. V. Harding. 1978. Gap junctions of chick lens fiber cells. *Exp. Eye Res.* 27:495–498.
27. Kuwabara, T. 1975. The maturation of the lens cell: a morphologic study. *Exp. Eye Res.* 20:427–443.
28. Landis, D. M. D., and T. S. Reese. 1981. Astrocyte membrane structure: changes after circulatory arrest. *J. Cell Biol.* 88:660–663.
29. Lecuyer, H., and D. G. Dervichian. 1969. Structure of aqueous mixtures of lecithin and cholesterol. *J. Mol. Biol.* 45:39–57.
30. Leeson, T. S. 1971. Lens of the rat eye: an electron microscope and freeze-etch study. *Exp. Eye Res.* 11:78–82.
31. Lowry, O. H., N. J. Rosebrough, A. L. Farr, and R. J. Randall. 1951. Protein measurement with the Folin phenol reagent. *J. Biol. Chem.* 193:265–275.
32. Luzzati, V., and F. Husson. 1962. The structure of the liquid-crystalline phases of lipid-water systems. *J. Cell Biol.* 12:207–219.
33. Makowski, L., D. L. D. Caspar, W. C. Phillips, and D. A. Goodenough. 1977. Gap junction structure. II. Analysis of the x-ray diffraction data. *J. Cell Biol.* 74:629–645.
34. Matsuto, T., and Y. Fujinaga. 1973. Scanning electron microscopic studies on the normal and senile cataractous human lenses. *Acta Soc. Ophthalmol. Jpn.* 77:853–872.
35. McIntosh, T. J., S. A. Simon, and R. C. MacDonald. 1980. The organization of *n*-alkanes in lipid bilayers. *Biochim. Biophys. Acta.* 597:445–463.
36. Nicholson, B. J., M. W. Hunkapiller, L. E. Hood, J.-P. Revel, and L. Takemoto. 1980. Partial sequencing of the gap junctional protein from rat lens and liver. *J. Cell Biol.* 87(2, Pt. 2):1539*a* (Abstr.).
37. Nir, S. 1976. Van der Waals interaction between surfaces of biological interest. *Recent Prog. Surf. Sci.* 8:1–58.
38. Okinami, S. 1978. Freeze-fracture replica of the primate lens fibers. *Albrecht v. Graefes Arch. Klin. Exp. Ophthal.* 209:51–58.
39. Peracchia, C. 1978. Calcium effects on gap junction structure and cell coupling. *Nature* (*Lond.*) 271:669–671.
40. Peracchia, C., and A. F. Dulhunty. 1976. Low resistance junctions in crayfish: structural changes with functional uncoupling. *J. Cell Biol.* 70:419–439.
41. Peracchia, C., and L. L. Peracchia. 1980. Gap junction dynamics: reversible effects of divalent cations. *J. Cell Biol.* 87:708–718.
42. Peracchia, C., and L. L. Peracchia. 1980. Gap junction dynamics: reversible effects of hydrogen ions. *J. Cell Biol.* 87:719–727.
43. Philipson, B. T., L. Hanninen, and E. A. Balazs. 1975. Cell contacts in human and bovine lenses. *Exp. Eye Res.* 21:205–219.
44. Portzehl, H., P. C. Caldwell, and J. C. Rugg. 1964. Calcium and the contraction of crab muscle fibers. *Biochim. Biophys. Acta.* 79:581–591.
45. Rae, J. L. 1979. The electrophysiology of the crystalline lens. *Curr. Top. Eye Res.* 1:37–90.
46. Robenek, H., and H. Greven. 1980. Orthogonal arrays of intramembranous particles in the basal plasma membranes of the epidermis of larval *Salamandra salamandra* (L.) (Amphibia, Urodela). *J. Ultrastruct. Res.* 72:119–122.
47. Takemoto, L. J., J. S. Hensen, and J. Horwitz. 1981. Interspecies conservation of the main intrinsic polypeptide (MIP) of the lens membrane. *Comp. Biochem. Physiol. B Comp. Biochem.* 68B:101–106.
48. Teller, D. C. 1976. Accessible area, packing volumes and interaction surfaces of globular proteins. *Nature* (*Lond.*) 260:729–731.
49. Waggoner, P. R., and H. Maisel. 1978. Immunofluorescent study of a chick lens fiber cell membrane polypeptide. *Exp Eye Res.* 27:151–157.
50. Wanko, T., and M. A. Gavin. 1958. The fine structure of the lens epithelium. *AMA Arch. Ophthalmol.* 60:868–879.

51. Weber, K., and M. Osborn. 1969. The reliability of molecular weight determinations by dodecyl sulfate-polyacrylamide gel electrophoresis. *J. Biol. Chem.* 244:4404–4412.
52. Wilkins, M. H. F., Blaurock, A. E., and Engelman, D. M. 1971. Bilayer structure in membranes. *Nat. New Biol.* 230:72–76.
53. Willis, N. R., M. J. Hollenberg, and C. R. Braekevelt. 1969. The fine structure of the lens of the fetal rat. *Can. J. Ophthalmol.* 4:307.
54. Zampighi, G. 1980. On the structure of isolated junctions between communicating cells. *In Vitro (Rockville).* 16(12):1018–1028.
55. Zampighi, G., J. M. Corless, and J. D. Robertson. 1980. On gap junction structure. *J. Cell Biol.* 86:190–198.
56. Zampighi, G., and P. N. T. Unwin. 1979. Two forms of isolated gap junctions. *J. Mol. Biol.* 135:451–464.
57. Zigler, J. S., and J. Horwitz, 1981. Immunological studies on the major intrinsic membrane polypeptides from human lens. *Invest. Ophthalmol. Visual Sci.* 21:46–51.